Article:
Ellis, M.O.A. orcid.org/0000-0003-0338-8920, Stamenova, M. and Sanvito, S. (2017) Multiscale modeling of current-induced switching in magnetic tunnel junctions using ab initio spin-transfer torques. Physical Review B, 96 (22). 224410. ISSN 2469-9950

https://doi.org/10.1103/physrevb.96.224410

Multiscale modeling of current-induced switching in magnetic tunnel junctions using *ab initio* spin-transfer torques

Matthew O. A. Ellis, Maria Stamenova, and Stefano Sanvito
School of Physics, AMBER and CRANN Institute, Trininty College, Dublin 2, Ireland
(Received 29 September 2017; published 7 December 2017)

There exists a significant challenge in developing efficient magnetic tunnel junctions with low write currents for nonvolatile memory devices. With the aim of analyzing potential materials for efficient current-operated magnetic junctions, we have developed a multi-scale methodology combining *ab initio* calculations of spin-transfer torque with large-scale time-dependent simulations using atomistic spin dynamics. In this work we introduce our multiscale approach, including a discussion on a number of possible schemes for mapping the *ab initio* spin torques into the spin dynamics. We demonstrate this methodology on a prototype Co/MgO/Co/Cu tunnel junction showing that the spin torques are primarily acting at the interface between the Co free layer and MgO. Using spin dynamics we then calculate the reversal switching times for the free layer and the critical voltages and currents required for such switching. Our work provides an efficient, accurate, and versatile framework for designing novel current-operated magnetic devices, where all the materials details are taken into account.

DOI: 10.1103/PhysRevB.96.224410

I. INTRODUCTION

Magnetic tunnel junctions (MTJs), composed of two epitaxially grown ferromagnetic (FM) metal layers separated by an insulating barrier (most often a few monolayers of MgO providing a dramatic spin-filtering enhancement), constitute the principle unit for a multitude of emerging technologies, in particular, in magnetic random access memory (MRAM) and spin torque oscillators (STOs) [1,2]. In both these cases the magnetization dynamics of the free FM layer is driven by a spin-polarized current. When the free-layer magnetization is misaligned with that of the polarizing layer, under current-carrying conditions, the exchange interaction between the itinerant and localized electron spins results in a spin-transfer torque (STT). For one of the two possible directions of the current this opposes the Gilbert damping torque and promotes switching from an antiparallel (AP) to a parallel (P) magnetization state or vice versa when the current direction is reversed [3]. For MRAM applications it is a significant challenge to develop MTJs with a suitably low write current so as to ensure energy efficiency and to prolong device lifetime [4].

It is becoming increasingly more apparent that computational modeling can provide an initial analysis of the viability of materials for efficient MTJs. However, a current-carrying MTJ, where magnetization dynamics is excited, poses a rather multiscale (both spatially and temporally) problem which cannot be fully tackled from the most fundamental *ab initio* theory. In fact, to date only a few studies have attempted to analyze a MTJ on multiple scales [5,6]. At one side, significant effort has been devoted to develop more precise *ab initio* models of spin-transfer torque [7,8]. These typically rely on ballistic quantum transport theory, which is suitable for the spin-transport properties of MTJs formed by epitaxially grown thin layers with atomically sharp interfaces and very few defects, such as in Fe/MgO/Fe. At the larger scale end, typical micromagnetic modeling of MTJs [9] employs Slonczewski's theory of STT [10]. This assumes perfectly symmetric junctions and incorporates all material-specific information of the electronic structure of the electrodes and their interfaces into a pair of polarization factors for the two FM leads, P_L and P_R. Such quantities are often taken as empirical parameters. Although the method may be suitable for some FeMgO-based MTJs, the interface details may be of crucial importance for other junctions (for instance, in antiferromagnetic stacks [11,12]). Atomistic spin dynamics (ASD) has proved useful in modeling systems on a finer detail than micromagnetics and has been developed to employ *ab initio* parameters to better describe the STT [13]. Still, there remains a significant gap in our modeling ability, since to date no quantitative and materials specific transport method has been combined with atomistic spin dynamics simulators. In practice, this means that we are not capable of performing current-induced spin dynamics simulations without making *a priori* assumptions on the nature and type of the STT.

In this work we attempt to bridge this gap and we present a multiscale approach to modeling current-induced magnetization dynamics in magnetic devices using STT. At the microscopic scale, a quantum transport method is employed to compute an *ab initio* atom-resolved STT, which is then mapped onto the Landau-Lifshitz-Gilbert (LLG) equation of motion for atomistic magnetic moments to perform the magnetization dynamics [14,15]. The method is general and can be applied to metallic and tunneling junctions on the same footing, including nanoscaled objects such as point contacts or atoms on surfaces.

Our paper is structured as follows: First we will introduce the computational scheme for calculating the *ab initio* STT and its mapping onto our atomistic spin model. We will then demonstrate this methodology on an example Co/MgO/Co/Cu MTJ stack. We will discuss the bias, current, and spatial dependence of the STT and how these features influence the magnetization switching of the free layer, both at zero and finite temperature.

II. METHODS

Our multiscale methodology is built upon using an *ab initio* method at the microscale for the electron transport and an atomistic scale spin model to simulate the dynamics.

In particular, we utilize the SMEAGOL [16,17] code to model ballistic electron transport through the MTJ under a finite-bias voltage. SMEAGOL is an implementation of the Keldysh nonequilibrium Green's function (NEGF) approach to the steady-state open-boundary problem within the framework of density functional theory (DFT), as implemented in the SIESTA code, which provides an efficient order-N scaling core DFT algorithm [18]. Within this formalism the MTJ is modeled as a central scattering region (SR) connected to two semi-infinite periodic leads. As the electronic properties of the latter can be determined independently from those of the junction, their action on the scattering region can be described in terms of suitably chosen self-energy operators acting at the SR boundaries. This effectively reduces the original electronic structure problem for an infinite nonperiodic system to an energy-dependent problem for a finite atomic construct. The bias voltage, V, is applied as a shift to the chemical potentials of either lead by $\pm V/2$, and the nonequilibrium charge density of the SR can be determined self-consistently from the associated nonequilibrium Keldysh Green's function.

For our calculation of the spin-transfer torque we follow the approach proposed by Haney *et al.* [11]. The out-of-equilibrium spin density $\boldsymbol{\sigma}^V$ is assumed to be separable into an equilibrium spin density $\boldsymbol{\sigma}^0$ and a transport correction $\boldsymbol{\sigma}^{\rm tr}$, where such correction is much smaller in magnitude than the equilibrium part. A transverse spin transport contribution arises from the noncollinearity in the open-boundary system, giving rise to a STT in the free layer. Further details of our method are given in Ref. [12]. Here we adopt the magnetic moment version (as opposed to working with spin variables) of the atom-resolved STT, in which the STT acting on the ath atom is written as

$$\mathbf{T}_a = \frac{\mu_{\rm B}}{2} \sum_{i\in a} \sum_j \boldsymbol{\Delta}_{ij} \times \boldsymbol{\sigma}^{\rm tr}_{ji} \,, \tag{1}$$

where $\boldsymbol{\Delta}_{ij}$ are the matrix elements of the exchange-correlation field written over the localized atomic basis orbitals of SIESTA and $\mu_{\rm B}$ is the Bohr magneton. Note that while the first summation is restricted to orbitals that belong to the atomic site a (the atom for which the torque is calculated), the second one spans over all the orbitals in the SR. The transport spin is calculated from the difference between the equilibrium ($V = 0$) and the nonequilibrium ($V \neq 0$) density matrices ρ^V_{ij} as

$$\boldsymbol{\sigma}^{\rm tr} = {\rm Tr}\left[(\rho^V - \rho^0)\boldsymbol{\sigma}\right] , \tag{2}$$

with $\boldsymbol{\sigma}$ being the vector of Pauli matrices.

The *ab initio* side of our multiscale approach is then completed with the evaluation of the dataset $\{\mathbf{T}_a(V,\theta)\}$ of atom-resolved STTs as a function of the bias voltage V and the angle θ between the fixed and the free-layer magnetizations. It should be noted here that the use of a single angular parameter assumes that there is no noncollinearity within the free layer. In some cases, when the self-consistent calculation of the density matrix across a range of finite-bias grid points is too involved computationally, we also utilize the linear response quantity, namely, the spin-transfer torkance (STTk) $\boldsymbol{\tau}_a$, that is defined as

$$\boldsymbol{\tau}_a \equiv \frac{\partial \mathbf{T}_a}{\partial V} = \frac{1}{2} \sum_{i\in a} \sum_j \boldsymbol{\Delta}_{ij} \times {\rm Tr}\left[\frac{\partial \rho_{ji}(V)}{\partial V}\boldsymbol{\sigma}\right]_{V=0} . \tag{3}$$

Once the spin-transfer torques, $\{\mathbf{T}_a(V,\theta)\}$, for the given junction are obtained, we can then proceed to computing the current-induced magnetization dynamics using an atomistic spin model. ASD is a semiclassical model typically using a Heisenberg spin Hamiltonian to describe a system of constant spin magnetic moments. These magnetic moments are localized at atomic sites and their dynamics is calculated from evolving discretized LLG-like equations of motion. The LLG equations for atomic spins with additional STTs are often referred to as LLG-Slonczewski equations, whose atomistic form reads

$$\frac{\partial \mathbf{S}_i}{\partial t} = -\gamma \mathbf{S}_i \times \mathbf{H}_i + \lambda \mathbf{S}_i \times \frac{\partial \mathbf{S}_i}{\partial t} + \frac{1}{\mu_i}\mathbf{T}_i(V,\{\mathbf{S}_i\}) \,, \tag{4}$$

where $\mathbf{S}_i = \boldsymbol{\mu}_i/\mu_i$ is a unit vector in the direction of the spin magnetic moment of atom i of magnitude $|\boldsymbol{\mu}_i| = \mu_i$. Since the *ab initio* torque in Eq. (1) is derived as the rate of change of the spin angular momentum, it is necessary to normalize the torque to the unit vector used in the ASD. In Eq. (4) λ is the atomistic damping parameter that corresponds to the Gilbert damping parameter at the microscopic scale and

$$\mathbf{H}_i(t) = -\frac{1}{\mu_i}\frac{\partial \mathcal{H}}{\partial \mathbf{S}_i} + \boldsymbol{\xi}_i(t) \tag{5}$$

is the effective magnetic field acting on spin i. The system is kept at a finite temperature through a stochastic time-dependent thermal field, $\boldsymbol{\xi}_i(t)$. In the white noise limit this is represented as a Gaussian random number with the following moments:

$$\langle \xi_{ia}(t) \rangle = 0 \,, \tag{6}$$

$$\langle \xi_{ia}(t)\xi_{jb}(t') \rangle = \frac{2\lambda k_B T}{\mu_s \gamma}\delta_{ij}\delta_{ab}\delta(t-t') \,, \tag{7}$$

where i,j label the different atoms, $a,b = x,y,z$ are the Cartesian components, and t,t' is the time. In order to model the dynamics of an MTJ free layer, we limit the Hamiltonian to contain only the Heisenberg exchange and a uniaxial anisotropy term as follows:

$$\mathcal{H} = -\sum_{ij} J_{ij}\mathbf{S}_i \cdot \mathbf{S}_j - \sum_i k_i(\hat{\mathbf{e}}_{\rm ani} \cdot \mathbf{S}_i)^2 \,, \tag{8}$$

where J_{ij} is the isotropic exchange constant and k_i is the uniaxial anisotropy constant for spin i along the axis $\hat{\mathbf{e}}_{\rm ani}$. In general one must also consider the demagnetizing field acting on the free layer and its contribution to the anisotropy. In the following we consider the intrinsic anisotropy to be out of plane ($\hat{\mathbf{e}}_{\rm ani} = \hat{\mathbf{z}}$), and since our free layer is ultrathin the demagnetizing field can be represented as that of an infinite thin platelet. Therefore, instead of calculating the demagnetizing field directly, which can be costly since it involves adding long-range dipolar interaction to the spin Hamiltonian, we incorporate it into the uniaxial field such that $k_i = k_u - \mu_0(M_s V_{\rm a})^2/2$. Here k_u is the intrinsic uniaxial

anisotropy constant, μ_0 is the permeability of free space, M_s is the saturation magnetization, and V_a is the atomic volume.

The next step is to map the two-parameter discretized *ab initio* $\{\mathbf{T}_a(V,\theta)\}$ dataset onto the STT term of Eq. (4), which is, in general, a continuous function of the angular coordinates of the whole set of spins $\{\mathbf{S}_i\}$. Such mapping can be performed in several manners, and here we have implemented three different strategies. The first is a full two-dimensional interpolation of the dataset, i.e., for each atom i in layer l_i an interpolated STT value is obtained for the specified voltage V and the instantaneous angle $\theta = \text{acos}(\mathbf{S}_i \cdot \hat{\mathbf{P}})$ between the local spin $\mathbf{S}_i$ and the direction of the fixed layer magnetization $\hat{\mathbf{P}}$. In order to simplify the calculation during the simulations, a linear interpolation is performed along V while a cubic spline is used for θ, since the dynamics is more sensitive to the angular variation and only a limited set of angles are calculated at finite voltage.

Our second mapping uses the angular dependence of the STT derived by Slonczewski [10]. In this way we avoid calculating the angular dependence of the STT at each voltage from first principles. The torque magnitude, however, is taken from the *ab initio* calculations, i.e., the bias dependence of the torque is still from first principles, namely, it is interpolated out of the *ab initio* dataset. This semifunctional mapping is given as

$$\mathbf{T}_i(V,\mathbf{S}_i) = T_{||}(V,l_i)\mathbf{S}_i \times \mathbf{S}_i \times \hat{\mathbf{P}} + T_{\perp}(V,l_i)\mathbf{S}_i \times \hat{\mathbf{P}}\,, \qquad (9)$$

where $T_{||}$ and $T_{\perp}$ are the parallel and perpendicular torque magnitudes, which can be extracted at $\theta = 90^{\circ}$.

Our final mapping utilizes the torkance instead of the finite voltage torques. In this manner a finite voltage is simulated by assuming a linear voltage dependence and by scaling the torkance to the desired V as follows:

$$\mathbf{T}_i(V,\mathbf{S}_i,l_i) = V\,\frac{\partial \mathbf{T}(\theta,l_i)}{\partial V}\bigg|_{V=0}\,. \qquad (10)$$

We discuss the applicability of this linear dependence in the case of a Co/MgO-based MTJ in the following section. The angular dependence can again be interpolated using cubic splines, but it is also possible to use the Slonczewski form given in Eq. (9).

Although the STTs are extracted from ballistic transport at a constant bias voltage, we have developed a numerical scheme to utilise the *ab initio*–calculated I-V characteristics, which allows us to simulate the atomistic spin dynamics also under constant-current conditions. As we will show in the next section, the conductance of a CoMgO-based MTJ is found to follow the equation

$$g(\theta,V) = \frac{J(V,\theta)}{V} = A(V) + B(V)\cos(\theta)\,. \qquad (11)$$

Our model can then compute the current as it changes with the free-layer angle and apply the torque appropriately for the given current and voltage. This is directly reflected in the prefactor of the Slonczewski STT equations [19].

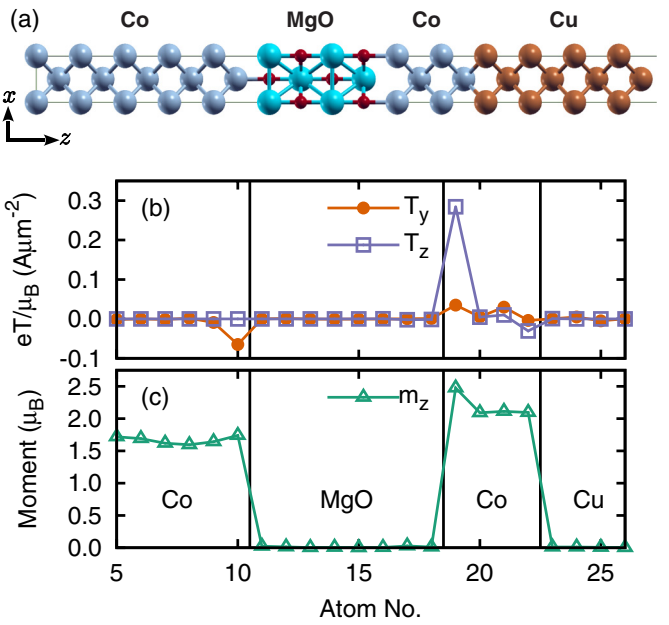

FIG. 1. The Co/MgO MTJ stack studied in this work. Panel (a) shows a schematic of the scattering region for the SMEAGOL calculation, while panels (b) and (c) present the atomic resolved *ab initio* STT for 90° misalignment at 1 V and the atomic spin moments profiles, respectively. In (b) and (c) the first 4 Co and last 4 Cu atoms are omitted, since in the calculations these are replaced with the semi-infinite leads.

III. RESULTS

A. *Ab initio* STT in a Co-MgO MTJ

Our computational strategy is now tested for a CoFeB-MgO based MTJ, which is probably the most studied magnetic device today. In order to model such a system, we simplify the structure to only comprise Co atoms in a Co/MgO(4)/Co(4)/Cu stack, where the numbers indicate the number of atomic planes in each layer. Note that the outermost layers are the semi-infinite leads as visualized in Fig. 1(a). In our generic Co-based MTJ, both leads share a bcc lattice with a lattice parameter of 2.857 Å. This is the lattice constant of Fe and the intention to mimic the highly spin-polarized conventional CoFeB lead.

Our DFT calculations are based on the local spin-density approximation with the Ceperley-Alder parametrization of the exchange-correlation functional as implemented in the SIESTA code [18]. A double-ζ numerical atomic basis set is used for all atomic species with additional polarization for s orbitals of the transition metal atoms. A Monkhorst-Pack Brillouin zone sampling is used, based on a 20×20 real-space grid.

The magnetic moments of each layer are shown in Fig. 1(c). As expected, there is no magnetization in MgO and Cu, while the Co fixed layer shows moments close to the bulk value of $\mu_{\text{Co}} = 1.72\mu_{\text{B}}$. Since the free layer is ultrathin, the moments are larger than in the bulk with a peak at the MgO interface. From the layer-resolved calculations we observe that the STT is strongly peaked at the MgO interface, as shown in Fig. 1(b) at 1 V for 90° misalignment. Following the sharp decay of the STT inside the Co layer, there is a characteristic higher STT

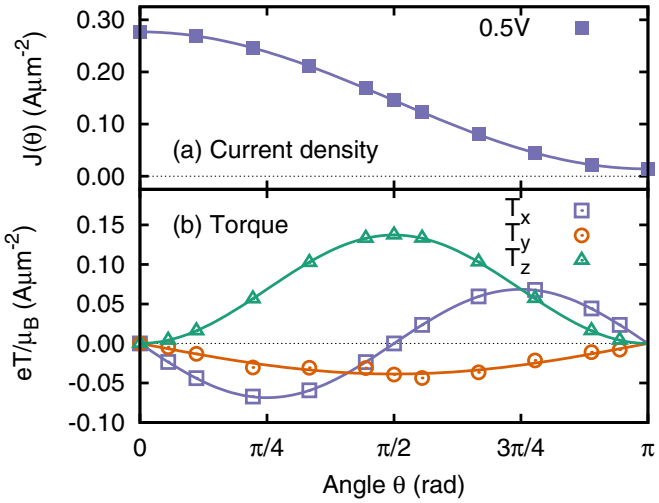

FIG. 2. The angular dependence of (a) the current density and (b) the total torque at 0.5 V. The solid line in (a) is a fit to the current density using $J(\theta) = A + B\cos(\theta)$. The solid lines in (b) are a fit using the Slonczewski angular dependence given in Eq. (9). In both cases the fits agree well with the data, indicating that the empirical forms can be used.

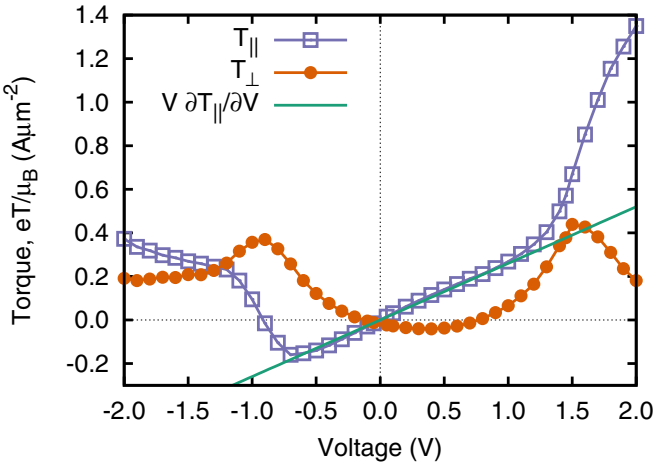

FIG. 3. The voltage dependence of the in-plane (open squares) and out-of-plane (filled circle) torque, and the in-plane torkance (solid line). The in-plane torque shows a linear behavior up to approximately 1.4 V. Within this range the torkance is a good approximation of the finite-bias torque. The out-of-plane torque shows a quadraticlike behavior, for which the zero-bias torkance is not sufficient to describe.

value also at the other interface with the Cu lead but with an opposite sign.

The angular dependence of the current density with the misalignment of the ferromagnetic layers is shown in Fig. 2(a) at $V = 0.5$ V. The solid line shows a fit obtained by using Eq. (11), which matches the data almost exactly and this behavior is consistent at higher voltages. Figure 2(b) shows the angular dependence of the total torque also at 0.5 V with the solid lines showing a fit using Eq. (9). Also in this case the fit performs well and so the functional approximation discussed earlier is a suitable replacement for the interpolation of the data. At higher voltages the perpendicular torque T_y becomes asymmetric, which would require a further parametrization. At present this asymmetry is neglected in the semifunctional mapping, since such torque contributes little to the switching so that its effect is minimal. We note that Slonczewski's description of the tunneling, which is based on Fermi's golden rule, is valid for sufficiently wide barriers, eliminating the direct overlap of the minority and majority spin states in the FM layers of symmetric MTJs [10]. As the STT decays very quickly from the interface and is practically contained within the free layer (see Fig. 1), Slonczewski's sinusoidal angular dependence of the net free-layer STT appears to be a good approximation for our junction (see Fig. 2).

Figure 3 shows the total STT acting on the free layer in the Co-MgO MTJ as function of the applied bias voltage for a fixed misalignment of the free-layer magnetization of 90°. The asymmetry of the torque with bias arises from the asymmetry of the stack, namely, the free layer contains only four atomic planes, while the fixed layer in our MTJ is semi-infinite. In both cases, however, there is an approximately linear and a quadratic relationship with voltage for the out-of-plane and in-plane torques, respectively. The slope of the in-plane STT around zero matches well our zero bias torkance from Eq. (3), and therefore the latter approximation offers a reasonable quantitative measure for the in-plane STT at low bias.

Figure 4 shows the current-voltage characteristics for our MTJ stack in both the parallel (P) and antiparallel (AP) configuration. The sharp increase of the in-plane STT above 1.4 V in Fig. 3 is due to the increase of the conductivity in the antiparallel configuration. This is in turn due to the fact that the Δ_1 symmetry band for the minority spin carriers is approximately aligned to the Δ_1 majority one at that bias voltage [5]. Intriguingly, while this leads to a lower tunneling magneto-resistance (TMR) at high voltages, the increased electron flow appears to result in a larger in-plane torque and in a reduction of the out-of-plane one, as can be seen in Fig. 3.

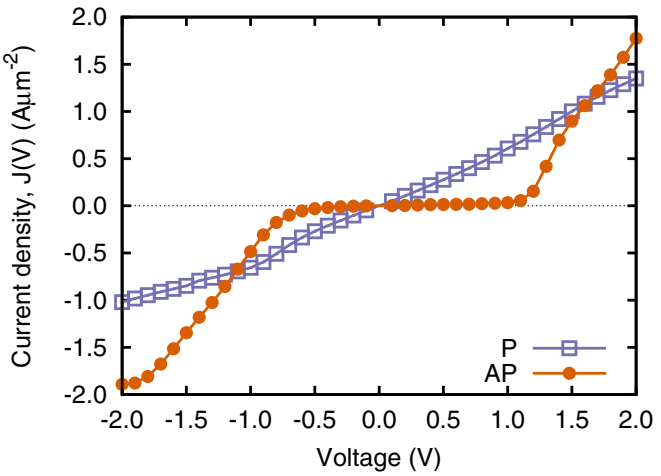

FIG. 4. The resulting current density for an applied bias voltage in the Co/MgO/Co/Cu MTJ. The solid circles show the current density in the antiparallel configuration, while the open squares show the parallel configuration. Up to approximately 1 V there is a significant TMR, but above this value more current flows in the antiparallel state and the TMR drops.

B. Switching dynamics at zero temperature

We now move our attention to the switching dynamics based on the *ab initio* torques computed in the previous section. In order to construct the spin model, we require values for the exchange constants, uniaxial anisotropy, atomistic Gilbert damping, and magnetic moments. For the exchange we use the tabulated bulk value [15] for bcc Fe, namely, $J_{ij} = 7.05 \times 10^{-21}$ J, which is assumed here to be similar to that of bcc Co, while the magnetic moments are taken directly from the SMEAGOL calculations. In order to explore a wide range of current-induced switching, we vary the anisotropy between 0.001 and 0.5 meV, which, as discussed earlier, accounts for both intrinsic anisotropy and demagnetizing fields. First-principles calculations by Hallal *et al.* [20] on Fe/MgO thin films found that the anisotropy is $k_u \approx 0.275$ meV per atom for a layer thickness similar to ours. For comparison the switching field at $k = 0.1$ meV is $H_k \approx 1.7$ T, while to achieve a thermal stability of $KV/k_B T_{\text{room}} = 60$ an area of $(36\ \text{nm})^2$ is required. The Gilbert damping in thin films has been observed to vary with the layer thickness, and the presence of capping layers can enhance the damping through spin pumping effects. Experimental measurements for a Ta/CoFeB/MgO stack show damping parameters of the order $\lambda = 0.01$ for ultrathin FM layers [21], and so here we vary the damping from 0.01 to 0.1. The magnetization dynamics is computed by numerically solving Eq. (4) using the stochastic Heun scheme [15] with a time step of 0.1 fs. This has been tested for stability in equilibrium.

We start by investigating the voltage required to observe switching in the MTJ free layer without explicit thermal effects. The lack of thermal effects allows us to simulate the switching with only the basic unit cell and periodic boundary conditions in the lateral directions. In order to measure the switching we calculate the time that is required for m_z to pass the $m_z = 0$ plane. We model the dynamics of each MTJ by initiating the simulation with a small deviation of the free-layer magnetization from the $-\hat{\mathbf{z}}$ axis at different applied bias voltages.

The magnetization switching curves are shown in Fig. 5 for (a) constant voltage and (b) constant current with an anisotropy of $k = 0.1$ meV and a damping parameter of $\lambda = 0.01$. When the junction is kept at a constant voltage the switching is uniform and stable. In practice, the magnetization of the free layer remains antiparallel to that of the pinned one for a long time and then switches fast. This is expected since the torque increases as the two magnetization vectors become noncollinear, and it is maximized for $\theta = 90°$. Furthermore, it is observed that increasing the voltage systematically shifts the transition to lower times.

In contrast, at a constant current the torque can initially overcome the anisotropy but, as the misalignment angle between the fixed and the free layer decreases, the resistance of the junction also decreases. This causes the voltage required to maintain the desired current to be reduced, and as a consequence, also the torque is reduced. The reduction of the torque as the magnetization vectors become noncollinear to each other has to be contrasted with an increase of the anisotropy, leading to a stable precessional state where a fine balance of the torques is achieved. As the current is increased further, the angle of this stable point becomes larger until it

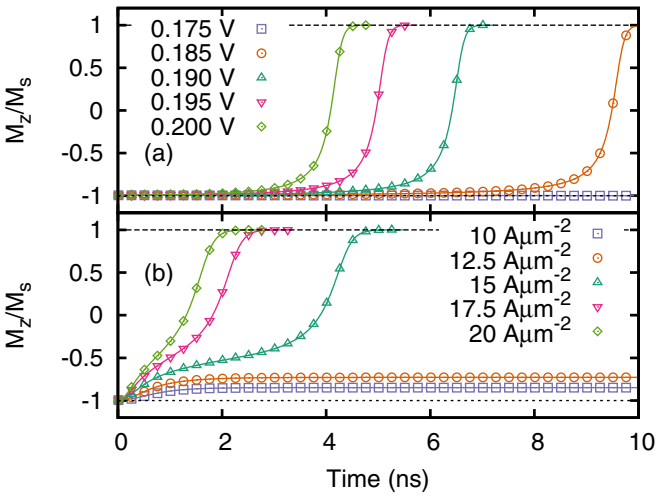

FIG. 5. Magnetization switching for a junction kept at (a) constant voltage and (b) constant current for $\lambda = 0.01$ and $k = 0.1$ meV. At constant voltage the switching is uniform above the critical voltage, while at constant current the torque has an additional angular dependence given by the variation of the conductivity (hence the voltage at constant current) with angle.

reaches the maximum of the anisotropy torque at about 45°. Then the full reversal occurs. Further increasing the current reduces the reversal time and also the transition width.

Figure 6 shows the measured switching time against the voltage calculated with the different mapping strategies for three values of the anisotropy. We find that there is no significant difference between the full and semi-interpolation methods, since the angular dependence of the *ab initio* STT agrees well with the Slonczewski form. As such, only the full interpolation results are compared to the torkance-based

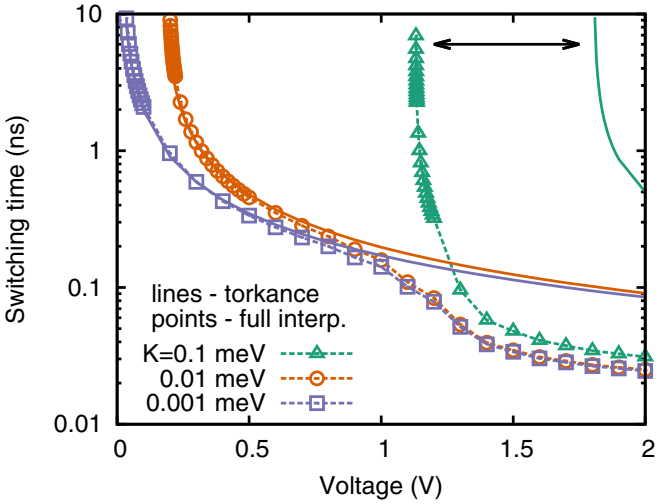

FIG. 6. The switching time for a Co free layer as a function of bias voltage for three values of the anisotropy and a damping coefficient of $\lambda = 0.1$. The open points are for calculations performed with the full interpolation, while the solid lines are for the torkance method and the dotted ones are a guide to the eye. The arrow indicates the difference between the torkance and full interpolation methods for the $k = 0.1$ meV case.

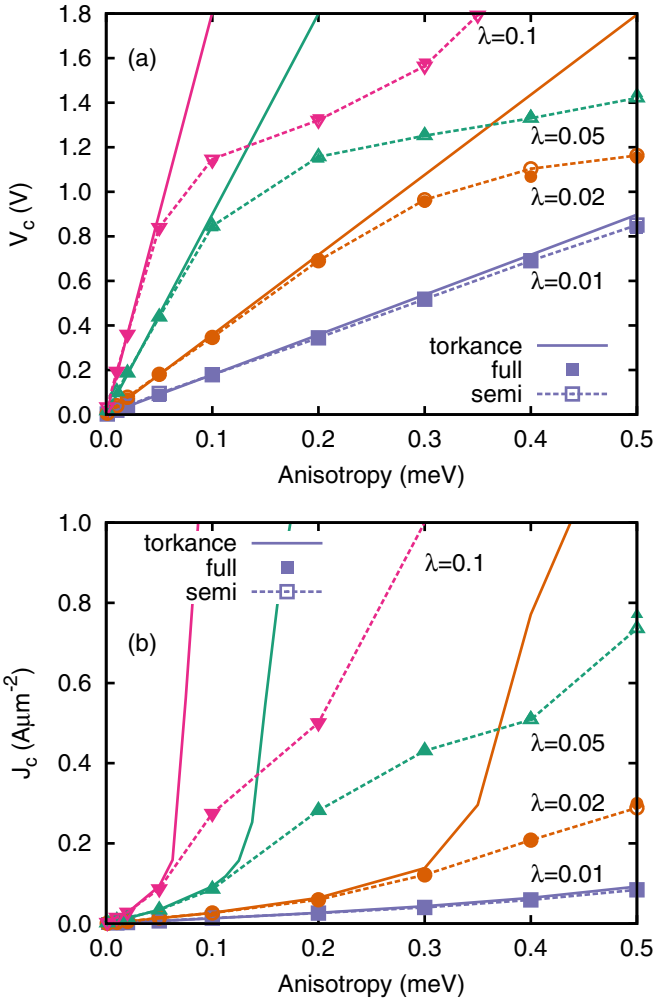

FIG. 7. The critical (a) voltage and (b) current required to switch the free layer for a given anisotropy and damping at $T = 0$ K. Three alternative methods for interpolating the STT are shown for each case: torkance (solid lines), full interpolation (filled circles), and semifunctional (open circles). The dotted lines are a guide to the eye.

ones. For each anisotropy there is no switching below a critical voltage and a sharp decay of the switching time above it. Since there is a large increase in the torque above approximately 1.4 V (see Fig. 3), the switching time shows a consistent drop at this point. For an anisotropy of 0.1 meV (green triangles and line), the critical voltage lies close to this increased torque and we find that there is a large difference between the calculations using the finite-voltage torques and those obtained at zero voltage with the torkance method.

The critical voltages and currents for a range anisotropy strengths and damping coefficients are shown in Fig. 7. The three interpolation methods discussed earlier are shown as solid lines for the torkance, filled points for full interpolation, and open points for the semifunctional method. Our results show that there is no significant difference between the semifunctional and the full interpolation method over the range simulated here. For the full interpolation method the loss of numerical accuracy may arise in some instances due to the poor interpolation at θ close to the end points, 0 and π, if too few data points are available where the curvature is high. Such numerical errors lead to longitudinal torques, which effectively (due to the constrained spin length in the ASD) reduce the net torque.

The nonlinear behavior of the critical voltage shown in Fig. 7(a) arises simply because of the calculated voltage dependence of the in-plane torque, while in (b) there is an additional effect arising from the voltage dependence of the current. At a lower damping the torkance matches the other methods for a wider range of anisotropies. This is due to the fact that the critical voltage is related to the product of the damping and the anisotropy. When the critical voltage is below approximately 1 V, then the torque is in the linear regime; hence, we find the torkance agrees well with the finite-voltage-calculated torque (see Fig. 3). In high-anisotropy systems, where a large switching voltage may be required, an accurate knowledge of the STT voltage dependence becomes important.

C. Switching dynamics at finite temperature

Finally, we consider the switching process at finite temperature. Now our simulation cell needs to be largely increased in order to account for the temperature-induced noncollinearity. In this case we simulate a $32 \times 32 \times 4$ spin slab corresponding to a lateral dimension of 9.2 nm and still apply periodic boundary conditions in the lateral directions. Ideally, one should consider thermal effects on the current and the STT as well, but here we only consider thermal effects in the ASD through the stochastic noise term introduced into the effective field in Eq. (5). The noncollinearity now requires a further decision to be made when mapping the STT to the ASD. The *ab initio* calculation of the torque is for a fully collinear free layer, but noncollinearity in ASD is required to achieve a thermal spin distribution. One can then decide to use the angle of the total magnetization or that of each individual spin in order to determine the torque. The effects of this choice will be discussed in what follows. Note that, in principle, one can still calculate the torques from *ab initio* for a noncollinear situation. In fact, one can even calculate the torques at each time step in the ASD, for instance, as it is done for the forces in *ab initio* molecular dynamics. This is, however, not practical here, since the transport calculations, in particular at finite bias, are much more demanding than the ASD ones.

Figure 8 shows the inverse average switching time at different temperatures for (a) $k = 0.1$ meV and (b) 0.5 meV. The filled symbols show results obtained by using the angle of the total magnetization to calculate the STT, while the open ones use the individual spin angle. From the figure we observe that results obtained with the different angle methods are almost indistinguishable from each other except in (b) at 300 K. Here the switching time is averaged over 24 independent simulations since it is a stochastic process. This may lead to an equivalence in the methods, since while these are fundamentally different the average switching time may be similar.

Different anisotropies present us two different situations. In Fig. 8(a) the inverse relaxation time is linear with the voltage, since the critical voltage is within the linear regime, while in Fig. 8(b) it is nonlinear. In general, however, for both anisotropy values increasing the temperature reduces the

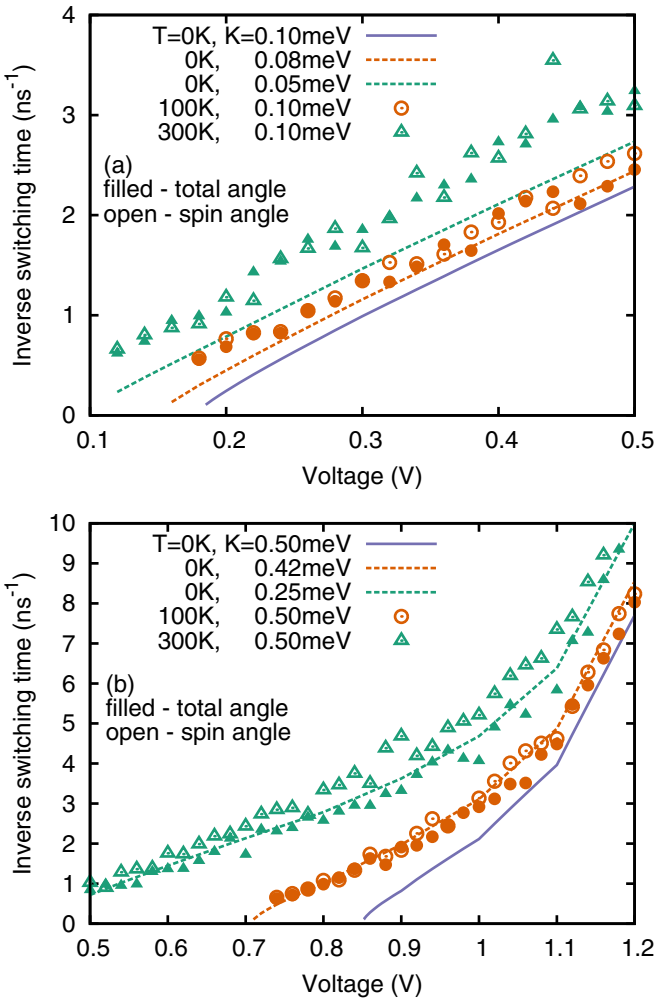

FIG. 8. Inverse switching time with (a) $k = 0.1$ meV and (b) 0.5 meV at $T = 0$ K (solid blue line), 100 K (orange circles) and 300 K (green triangles). Filled and open symbols represent simulations run by using the angle calculated for the total magnetization or for each individual spin, respectively. The dashed lines indicate the inverse reversal time at $T = 0$ K using a scaled anisotropy constant.

switching time and also the critical voltage. Within a micromagnetic picture this behavior is reproduced by introducing temperature-dependent parameters, namely, the anisotropy, the damping, and the magnetic moment. These reduced parameters then lead to a reduction in the critical switching voltage. Callen-Callen theory [22] predicts that at finite temperature the macroscopic uniaxial anisotropy constant K_u scales as $K_u(T)/K_u(0) = [M(T)/M(0)]^3$. From our simulations we find that at 100 K and 300 K the average magnetization is approximately 0.94 and 0.80, respectively. This returns us expected anisotropy constants of $K_u(100) \approx 0.83K_u(0)$ and $K_u(300) \approx 0.51K_u(0)$. The dashed lines in Fig. 8, therefore, show the inverse switching time at 0 K obtained by using these scaled anisotropy values. As we can see in panel (b), the zero-temperature dynamics computed using these scaled constants agree well with the average switching time obtained at finite temperature, despite the lack of thermal fluctuations. The same is not true for the lower-anisotropy case of Fig. 8(a). Here there is agreement only at higher voltages for 100 K, while at 300 K the zero-temperature switching times at the rescaled anisotropies are constantly longer than those obtained with the finite-temperature dynamics. This has to be attributed to the actual thermal fluctuations, which are more pronounced for a lower anisotropy and cause the switching to occur faster.

IV. CONCLUSION

To summarize, we have developed a multiscale modeling methodology combining *ab initio* calculations of the spin-transfer torque and large-scale finite-temperature spin dynamics simulations. Using the SMEAGOL code, both the STT and the linear response STTk have been computed for various applied voltages and angles of misalignment between the fixed and free magnetic layer in a nanoscopic junction. This is then mapped onto an atomistic spin dynamics model, which is used to calculate the switching times with and without thermal effects. We apply this methodology to a prototype MTJ based on Co/MgO, where we find that the STT is strongly localized on the Co atoms at the MgO interface and that the STT is linear at low voltages. In contrast, above 1.4 V there is a sharp increase in the total current in the AP configuration driven by the minority spin component. Such current density increase leads to a sharp enhancement of the in-plane torque and in a reduction of the out-of-plane one.

The *ab initio* calculated torques are then mapped onto the ASD with different mapping types being analyzed. A full interpolation of the *ab initio* data set is preferred, but using the Slonczewski angular form together with the *ab initio* voltage dependence extracted at a fixed angle performs equally well over a wide range of parameters. Due to the linear nature of the STT, at low bias the 0-V linear response (torkance) is a suitable replacement. At finite temperature the picture described above does not change drastically, except for the fact that the thermal fluctuations reduce the critical voltage required for switching.

The advantage of such multiscale methodology is that no empirical model of the STT is required, as this is calculated at the atomic level from first-principles ballistic transport theory. The atomic resolution allows systems where the typical micromagnetic models break down (e.g., where atomically staggered magnetic order is present) to be investigated. While currently some parameters, such as the exchange interaction and the anisotropy, are inferred from experiments, those can also be taken from *ab initio* calculations of the actual MTJ stack with atomic resolution [20,23]. Computational feasibility may ultimately limit the size of treatable systems and the accessible time scales; however, this prototypical MTJ study is still far from these limits, suggesting a range of realistic magnetic multilayered devices (including some accounts for disorder) to be well within the scope of the method.

ACKNOWLEDGMENTS

This work has been supported by the Science Foundation Ireland Principal Investigator Award (Grants No. 14/IA/2624 and No. 16/US-C2C/3287). We gratefully acknowledge the DJEI/DES/SFI/HEA Irish Centre for High-End Computing (ICHEC) for the provision of computational facilities. We also acknowledge the Trinity Centre for High Performance Computing (TCHPC) for use of computational resources.

[1] A. Brataas, A. D. Kent, and H. Ohno, Nat. Mater. **11**, 372 (2012).
[2] D. C. Ralph and M. D. Stiles, J. Magn. Magn. Mater. **320**, 1190 (2008).
[3] J. Slonczewski, J. Magn. Magn. Mater. **159**, L1 (1996).
[4] R. L. Stamps, S. Breitkreutz, J. Åkerman, A. V. Chumak, Y. Otani, G. E. W. Bauer, J.-U. Thiele, M. Bowen, S. a. Majetich, M. Kläui, I. L. Prejbeanu, B. Dieny, N. M. Dempsey, and B. Hillebrands, J. Phys. D **47**, 333001 (2014).
[5] Y. Xie, I. Rungger, K. Munira, M. Stamenova, S. Sanvito, and A. W. Ghosh, in *Nanomagnetic and Spintronic Devices for Energy-Efficient Memory and Computing* (John Wiley & Sons, Ltd., Chichester, UK, 2016), pp. 91–132.
[6] Y. Xie, J. Ma, S. Ganguly, and A. W. Ghosh, J. Comput. Electron. (2017), doi: 10.1007/s10825-017-1054-z.
[7] C. Heiliger and M. D. Stiles, Phys. Rev. Lett. **100**, 186805 (2008).
[8] P. M. Haney, D. Waldron, R. A. Duine, A. S. Núñez, H. Guo, and A. H. MacDonald, Phys. Rev. B **76**, 024404 (2007).
[9] D. V. Berkov and J. Miltat, J. Magn. Magn. Mater. **320**, 1238 (2008).
[10] J. C. Slonczewski, Phys. Rev. B **71**, 024411 (2005).
[11] P. M. Haney, D. Waldron, R. A. Duine, A. S. Núñez, H. Guo, and A. H. MacDonald, Phys. Rev. B **75**, 174428 (2007).
[12] M. Stamenova, R. Mohebbi, J. Seyed-Yazdi, I. Rungger, and S. Sanvito, Phys. Rev. B **95**, 060403 (2017).
[13] J. Chureemart, R. Cuadrado, P. Chureemart, and R. Chantrell, J. Magn. Magn. Mater. **443**, 287 (2017).
[14] M. O. A. Ellis, R. F. L. Evans, T. A. Ostler, J. Barker, U. Atxitia, O. Chubykalo-Fesenko, and R. W. Chantrell, Low Temp. Phys. **41**, 908 (2015).
[15] R. F. L. Evans, W. J. Fan, P. Chureemart, T. A. Ostler, M. O. A. Ellis, and R. W. Chantrell, J. Phys.: Condens. Matter **26**, 103202 (2014).
[16] A. R. Rocha, V. M. García-Suárez, S. Bailey, C. Lambert, J. Ferrer, and S. Sanvito, Phys. Rev. B **73**, 085414 (2006).
[17] I. Rungger, O. Mryasov, and S. Sanvito, Phys. Rev. B **79**, 094414 (2009).
[18] J. M. Soler, E. Artacho, J. D. Gale, A. García, J. Junquera, P. Ordejón, and D. Sánchez-Portal, J. Phys.: Condens. Matter **14**, 2745 (2002).
[19] J. C. Slonczewski and J. Z. Sun, J. Magn. Magn. Mater. **310**, 169 (2007).
[20] A. Hallal, H. X. Yang, B. Dieny, and M. Chshiev, Phys. Rev. B **88**, 184423 (2013).
[21] S. Iihama, Y. Sasaki, H. Naganuma, and M. Oogane, J. Phys. D **49**, 35002 (2015).
[22] E. R. Callen and H. B. Callen, Phys. Rev. **129**, 578 (1963).
[23] C. J. Aas, P. J. Hasnip, R. Cuadrado, E. M. Plotnikova, L. Szunyogh, L. Udvardi, and R. W. Chantrell, Phys. Rev. B **88**, 174409 (2013).